

Imputing Rainfall Data for Flood Simulation in Citarum River, West Java

Muhammad Yoga Pratama¹, Stevanus Nalendra Jati^{1*}, Muhammad Rendana²

¹Study Program of Geological Engineering, Universitas Sriwijaya, Indonesia

²Department of Chemical Engineering, Universitas Sriwijaya, Indonesia

*Corresponding Author: s.nalendra@unsri.ac.id

Article history

Received 30 July 2021	Received in revised form 15 July 2022	Accepted 7 March 2023	Available online 11 March 2023
--------------------------	--	--------------------------	-----------------------------------

Abstract: The central role of the Citarum River as a buffer to meet the needs of agricultural irrigation, industrial activities, and raw water in the six surrounding districts, including 80% of the population of Jakarta, has experienced a decline in conditions from up-downstream. That way, a lot of data is available regarding the adaptation of floods, drought, and other water source functions for an integrated concept for Citarum. The focus of the study is in the Central Citarum Zone by using 5 and 10 years of rainfall intensity (time series), actualizing the runoff coefficient, Intensity Duration Frequency (IDF) modeling to the formulation of the peak runoff discharge. This achievement is realized by applying Gumbel's Method and Mononobe's Equation and optimizing the 2D HEC-RAS software. Experimental data from 2010 to 2019 indicated that November was the highest rainfall of 448.07 mm/hour, while the lowest was in July with a value of 52.50 mm/hour. The simulation results show an increase in flow rate up to 11%, which means it affects the river's capacity to accommodate the overflow load. Furthermore, this simulation is equipped with a map of the flood-affected areas with a peak discharge scenario in November.

Keywords: Citarum River, rainfall, runoff coefficient, discharge, and flood

1. Introduction

Floods are natural disasters that often occur in Indonesia, especially in West Java Province, caused by high rainfall and changes in the function of the landform [1]-[2]. High rain will affect the surface runoff in the river. Meanwhile, changes in land shape will significantly affect water catchment areas [3]-[4]. The Citarum River is the main river that passes through West Java Province (Fig. 1). This river overflow caused flooding in West Java Province.

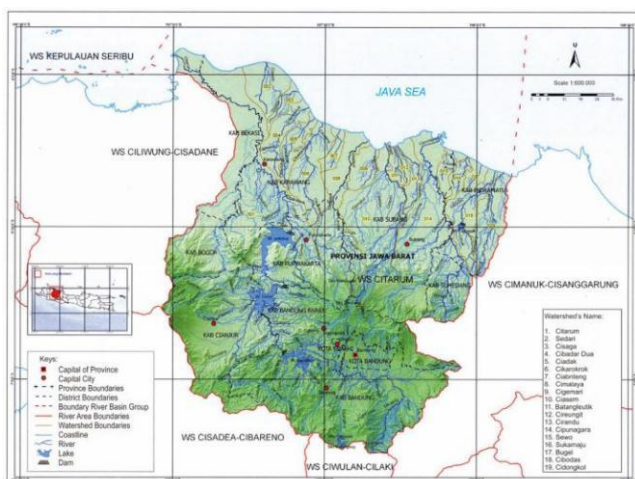


Figure 1. Location of the study area, upstream in the south and the river flows to the north.

The Citarum River is the longest and largest river in West Java Province. The river flows to the west, passing Majalaya and Dayeuhkolot. Then it turns northwest and north, becoming the border between Cianjur Regency and West Bandung Regency, passing

through Purwakarta Regency, and ending in Karawang Regency [2]. The Citarum River is helpful as a fishery resource for residents, and its flow also acts as a reservoir for electricity generation and irrigation. This research focuses on the Citarum River in the Central Citarum Zone, which connects the Saguling Reservoir and Cirata Reservoir, located in West Bandung Regency and Cianjur Regency, West Java Province.

The thing that affects flooding is the high intensity of rain which causes surface runoff discharge. Other factors, namely change in land cover, type of lithology, and slope, also affect flooding. Based on these factors, this study aims to model the intensity of rainfall from 2010 to 2019 and calculate the estimated peak runoff discharge in the 5- and 10-year return period (time series), which is then processed using the HEC-RAS (Hydrologic Engineering Center-River Analysis System) software to obtain flood-prone areas in the Citarum River in the Central Citarum Zone, linking the Saguling Reservoir and the Cirata Reservoir [5].

Rainfall data uses intensity adopted from SiBias software [6], through climate change scenarios Representative Concentration Pathway (RCP) 8.5. Climate projections respond to climate change to global warming caused by emissions of greenhouse gases and other pollutants. To project the climate in 2100, [7] has introduced several new climate change scenarios, namely the RCP scenario consisting of RCP 2.6, RCP 4.5, RCP 6.0, and RCP 8.5. To understand the system's processes and climate change, optimize a (Global Circulation Model) or a Regional Climate Model (RCM). Application of rainfall data to find the flow rate plan [6]-[7].

Surface runoff is rainwater that flows above the soil

surface, which transports soil substances and particles [8]-[9]. Runoff occurs due to the intensity of rain that falls beyond the infiltration capacity. When the infiltration rate reaches peak capacity, water will fill the basins on the ground surface. The runoff coefficient is highly dependent on data on land cover, soil type, and slope [9]-[10].

Significant changes in land cover are the main factors causing the increased runoff coefficient, and the risk of water runoff will be even greater [8]-[9]. Changing land cover patterns can significantly affect waterways, change water quality, and create new floodplains. The dynamics of land cover in the upstream part significantly impact the downstream, namely low precipitation, which increases the potential risk of flooding.

The type of soil/rock can affect the amount of runoff coefficient in an area. The kind of rock in a room will affect the speed of water infiltrating into the rock and soil infiltration [11].

The slope is a parameter that determines the value of the runoff coefficient. The slope level affects the size of the soil infiltration capacity and can determine the velocity of rainwater flow through the ground to the basin (river/lake).

2. Material and Methods

2.1. Materials

This study optimizes secondary data sourced from various ministries and state agencies (K/L). Then apply integration with primary data from field measurements as a form of model validation and verification. Some secondary data and the source of the license include:

- Digital elevation model (DEM) by the Geospatial Information Agency (BIG). For topography and slope visualization, see <https://tanahair.indonesia.go.id/demnas/#/>.
- Land cover from the WebGIS of the Ministry of Environment and Forestry (KLHK), see <http://webgis.menlhk.go.id:8080/pl/pl.htm>.
- Rainfall data from Saguling Station, Cirata Station, and Cianjur Station, 2010-2019 time series, from SiBias running [6], to calculate rainfall intensity and planned flow rate.

2.2. Methods

2.2.1. Rainfall analysis

The purpose of rainfall analysis is to determine the maximum average rainfall in a specific return period to calculate the estimated peak runoff discharge [12]-[13]. The stages of processing rainfall data go through three stages, including analysis of the maximum annual rainfall [14]. Data comes from SiBias in the form of daily rainfall data using the Gumbel Method. Data visualization with Intensity Duration Frequency (IDF) curve on Mononobe time series 5 and 10 years [15]-[17]. The Gumbel method

aims to analyze the possible intensity of rainfall with the desired return period [18], the Gumbel's formula (Equation 1), according to [19]-[21], is written as follows:

$$X = \bar{X} + K.S \quad K = \frac{Y_{Tr} - Y_n}{S_n}$$

$$Y_{Tr} = -\ln \left[-\ln \frac{Tr-1}{Tr} \right] \dots \dots \dots (1)$$

Where:

- X : The intensity of rainfall on the duration and specific return period;
- \bar{X} : Average maximum rainfall from the data;
- K : frequency factor for the analysis of opportunities;
- YTr : Variance reduction factor;
- Yn : The average value of the variance;
- Sn : Standard deviation of variance;
- Tr : The return period of rain.

The analysis of rain intensity using daily rainfall data must be converted to rain intensity into a specific time (5, 10, 15, 30, 60, 120, 240, 360, 720 minutes) using the Mononobe's formula (Equation 3).

$$I = \frac{R_{24}}{24} \left[\frac{24}{t} \right]^{2/3} \dots \dots \dots (2)$$

Where:

- I : Rainfall intensity (mm/hour);
- R₂₄ : Rainfall duration (minute);
- t : Maximum rainfall on the specific return period.

Next, build a model of the IDF curve for time series 5 and 10 years through selection from three equations (Equation 3-5), referring to the slightest difference between the results and the calculation of rainfall intensity using the Gumbel Formula. Determination of rain intensity (I) in various return periods can be through [11], namely:

$$I = \frac{a}{t+b}$$

$$a = \frac{\sum[I.t]\sum[I^2] - \sum[I^2.t]\sum[I]}{N\sum[I^2] - \sum[I]^2}$$

$$b = \frac{\sum[I]\sum[I.t] - N\sum[I^2.t]}{N\sum[I^2] - \sum[I]^2} \dots \dots \dots (3)$$

$$I = \frac{a}{t^n}$$

$$\log a = \frac{\sum[\log I]\sum[(\log t)^2] - \sum[\log t \cdot \log I]\sum[\log t]}{N\sum[(\log t)^2] - \sum[\log t]^2}$$

$$n = \frac{\sum[\log I]\sum[\log t] - N\sum[\log t \cdot \log I]}{N\sum[(\log t)^2] - \sum[\log t]^2} \dots \dots \dots (4)$$

$$I = \frac{a}{\sqrt{t+b}}$$



$$a = \frac{\sum[I \cdot \sqrt{t}] \sum[I^2] - \sum[I^2 \cdot \sqrt{t}] \sum[I]}{N \sum[I^2] - \sum[I]^2}$$

$$b = \frac{\sum[I] \sum[I \cdot \sqrt{t}] - N \sum[I^2 \cdot \sqrt{t}]}{N \sum[I^2] - \sum[I]^2} \dots \dots \dots (5)$$

Where:

- I : Rainfall intensity (mm/hour);
- a, b, and c : Constants, depending on the duration of rainfall in a region;
- t : Rainfall duration (minute).

2.2.2. Analysis of runoff coefficient

There are three main aspects to determining the value of the runoff coefficient, namely land cover, lithology, and slope [8]. The calculation of these three aspects uses the Hassing Method with the weight of each assessment from each element (Table 1). Then, the runoff coefficient value becomes a component in the design flow discharge formula (Equation 6).

Table 1. The runoff coefficient using the Hassing’s Method (modified [11]).

Land Cover (CL)	CL Value	C
Shrubs	0.07	
Rice Field	0.15	
Swamp bush	0.07	
Residential	0.6	
Open Space	0.2	
Plantation	0.4	
Dryland farming	0.1	
Secondary dryland forest	0.2	
Dryland farming mixed with shrubs	0.1	
Lithology (CS)	CS Value	
Qs (loose material: sand, silt, clay)	0.16	
Qa (loose material: bolder, gravel)	0.04	
QTK (pyroclastic rock layers)	0.26	
Tmpm (fine-grained sedimentary rock)	0.26	
Tma (fine-grained sedimentary rock)	0.26	
Slope Classification (CT)	CT Value	
Flat (< 1%)	0.03	
Very Ramps (2- 10%)	0.08	
Ramps (11-20%)	0.16	

2.2.3. Estimating of peak discharge

The calculation of the estimated peak runoff discharge uses a rational method because the area of the study area is not more than 1000 km² or as large as 169 km². The following is an equation of the rational method:

$$Q_{max} = 0,002778 \cdot C \cdot I \cdot A \dots \dots \dots (6)$$

Where:

- Q_{max} : Peak/maximum discharge (m³/sec);
- C : Surface runoff coefficient (0 ≤ C ≤ 1);
- I : Rain intensity (mm/hour);
- A : Size of stream area (km²).

3. Result

3.1. Rainfall Intensity

The maximum average monthly rainfall data processing results for the 2010-2019 time series indicate that November is the peak intensity with rain reaching 448.07 mm/hour (Fig. 2). Meanwhile, low rainfall intensity occurred in July, which was only 52.5 mm/hour. Referring to these results and being integrated with hydrometeorology, July becomes the dry season and impacts drought [22]. On the other hand, November needs to be aware of the impact of intense rain, namely floods. Disasters, the research location has no implications for forest fires because the dominant lithological factor is not composed of organic carbon material. However, the potential for flooding is possible. So this study looks deeper into areas with the potential for flooding from a rainfall perspective [23].

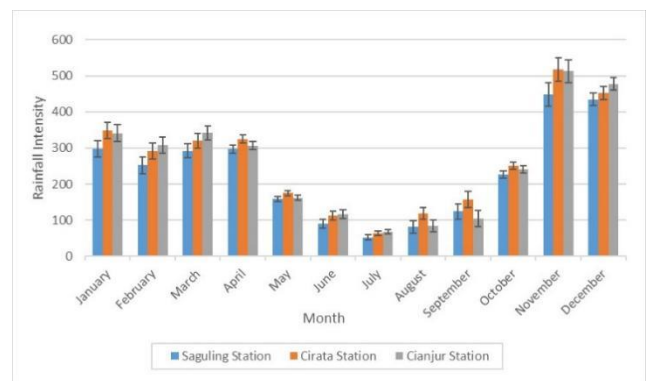


Figure 2. Monthly average of maximum rainfall from three stations, eg: Saguling Station (blue), Cirata Station (orange), and Cianjur Station (grey).

Calculating the Gumbel method (see Eq. 1), the results indicate an increase in rainfall along with an increase in return periods. Furthermore, the calculation results of the Mononobe Equation play a role in converting rainfall intensity in 10-time durations, which then becomes a component in the estimation of peak runoff discharge [7],[15]. The Intensity Duration Frequency (IDF) curve shows that high rainfall intensity occurs for a short duration (Fig. 3). This indicates that rain with a high intensity often referred to as heavy rain, generally lasts for a short time. However, it is different from rainfall with low intensity, which usually lasts for quite a long duration [24]. The calculation of rainfall intensity becomes a multiplying factor in calculating the peak runoff discharge using the Rational Method [7]-[8]. The results of the calculation of rainfall intensity, a rainfall intensity map model was built. The red color represents that the area has a high rainfall intensity and is getting to the green color, indicating the lower rainfall intensity, as shown in Appendix 1.

3.2. Runoff coefficient

Land cover change through GIS-based spatial analysis (Appendix 2). Expansion occurred in the industrial forest (light green), settlement (black), and

significantly dryland farming with shrub (cream) which reached 11 km². Meanwhile, the rest is relatively reduced or lost has changed into other land functions, especially openland (purple), which has drastically changed up to 8 km² (Table 2). Significant changes in land cover are found in open land, which is transformed into dry land agricultural land with shrubs. This affects the critical water catchment area. Furthermore, rice fields are turned into residential land and industrial plantations. Each landform has a different coefficient value (Table 3).

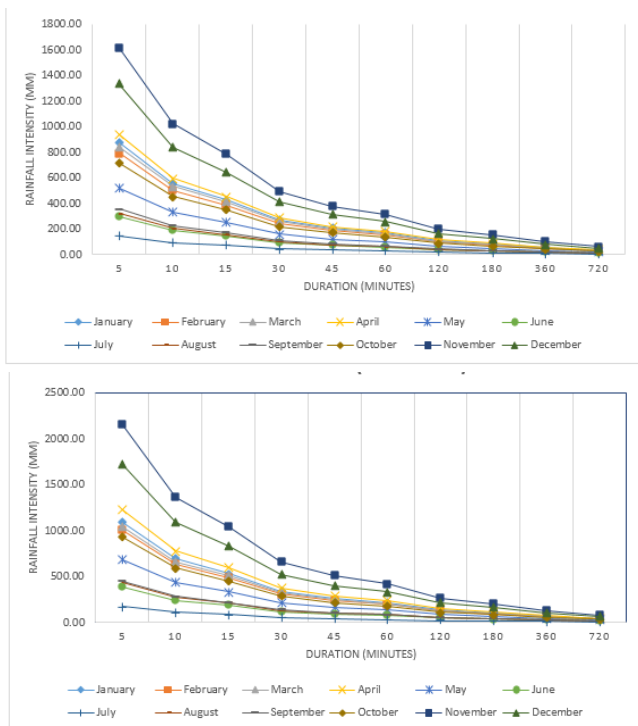


Figure 3. The IDF curve of the mean from the three stations over the time series return period, eg: 5 year (top) and 10 year (bottom).

Table 2. Land cover type-extend in the study area.

Land Cover	2014 (km ²)	2019 (km ²)
Industrial forest (If)	30	32
Dryland farming (Df)	36	35
Farm (F)	7	7
Dryland farming with shrubs (Dfws)	4	15
Openland (O)	19	11
Rice field (Rf)	58	52
Settlement (S)	8	10

The following parameter in the Hassing method is the type of lithology shown in Appendix 3 in the form of a geological map of the research area. The study area is dominated by volcanic rocks classified into sand and gravel in the Hassing classification. These rocks consist of the young Mt. Gede, the old Volcano, and the Pb Formation, an area of 93 km², and there is a Quarter Alluvium with an area of 5 km². Then, clastic sedimentary rocks that are carbonic, namely the Mt Formation, Cantayan Formation, Jatiluhur Formation,

Citarum Formation, and Rajamandala Formation, are classified into rock layers in the Hassing classification. In Table 4, the Hassing classification shows that the coefficient values of sand and gravel and rock layers have different values and have an area of 62 km².

The third parameter in the Hassing method is the slope level. In the study area, the types of slopes are divided into 3, namely very gentle (2 to 10%), mild (11 to 20%), and steep (> 20%), which have different coefficient values. In Figure 8, you can see slopes with different types. Very gentle slope dominates the research area by 43%, followed by gentle slope types 35% and steep 22%, whose area can be seen in Table 5 and Appendix 4.

Table 3. Runoff coefficient of land cover parameters.

Ye	Para	Land Cover						
		If	Df	F	Dfws	O	Rf	S
2014	A	30	36	7	4	19	56	8
	C	0.2	0.1	0.4	0.1	0.2	0.15	0.6
	C.A	6	3.6	2.8	0.4	3.8	8.4	4.8
	CL	0.19						
2019	A	32	35	7	15	11	50	10
	C	0.2	0.1	0.4	0.1	0.2	0.15	0.6
	C.A	6.4	3.5	2.8	1.5	2.2	7.5	6
	CL	0.19						

Table 4. Runoff coefficient of lithology parameters.

Lithology	A	C	C.A	CS
Alluvium (sand-gravel)	5	0.16	0.8	
Old Volcano (sand-gravel)	35	0.16	5.6	
Young Volcano (sand-gravel)	30	0.16	4.8	
Pb Fm. (sand-gravel)	28	0.16	4.48	
Mt Fm. (rock layers)	9	0.26	2.34	0.2
Cantayan Fm. (rock layers)	2	0.26	0.52	
Jatiluhur Fm. (rock layers)	9	0.26	2.34	
Citarum Fm. (rock layers)	30	0.26	7.8	
Rajamandala Fm. (rock layers)	12	0.26	3.12	
	160		31.8	

Table 5. Runoff coefficient of lithology parameters.

Slope	A	C	C.A	CT
Very Sloping	69	0.08	5.52	
Sloping	56	0.16	8.96	0.15
Steep	35	0.26	9.1	
	160		23.58	

Based on the land cover parameters, rock/soil type, and slope, all coefficient (C) values were accumulated, and the result was 0.54. This means that the potential for water overflowing in the Citarum River area of the Central Citarum Zone is 54%. Furthermore, the added coefficient (C) is used to find the estimated peak discharge value.

3.3. Discharge plan

Based on the rainfall intensity data, multiplied by the runoff coefficient value, the area of the study area (see Eq. 6), the planned flow discharge value is shown in Fig. 4. The designed flow discharge value obtained shows an

increase in the estimated peak discharge for the 5-10 years period of 11.2%. The planned flow rate data that has been obtained are then processed again into the HEC-RAS software so that it can identify flood-prone areas [1],[4],[25]-[26].

3.4. Flood simulation

Based on the flood hazard map that has been created using HEC-RAS software (Fig. 5), the area in red is the flood runoff area, while on the flood-prone zoning map, the area in yellow is the flood-prone area that has been zoned. As can be seen on the map, the flood-prone areas along the river have a different location [12],[27]-[28]. This is caused by several factors, namely topographic conditions, slope level, and river geometry. The river geometry includes the river's width, the cross-sectional height of the river, and the cross-sectional area of the river [20],[29]. Also, another very influential thing is the erosion level of the river, which affects the formation of the river [30].

The delineation map of flood-prone areas in the study area is divided into three segments: the upstream segment, the middle segment, and the downstream

segment, which are based on flood vulnerability in the study area. In the upstream part, the level of flood hazard is low. This is because the slopes in this segment are included in the steep category ($> 20\%$), and the topography is classified into high hills, namely 500-1000 masl [25],[30]. The erosional level in this segment is low, which is indicated by the absence of river meandering. Furthermore, there is the middle segment that has a high level of flood vulnerability. This is because it has a low topography, namely 150-500 masl, which belongs to the hilly and low hilly category [25],[31]. This segment has very gentle slopes (2-10%), which dominates, and there is also a gentle slope (11-20%), which has a high erosion level marked by river meandering. Meandering of the river is what causes this segment to have a high level of flood vulnerability. Finally, there is a downstream segment that has a very gentle slope (2-10%) to sloping (11-20%). This segment is located at an altitude of 150-500, which is included in the classification of a low hill to hilly [10]-[11],[25],[30]-[31], which has a relatively moderate erosion level, due to the river bends that are not too steep.

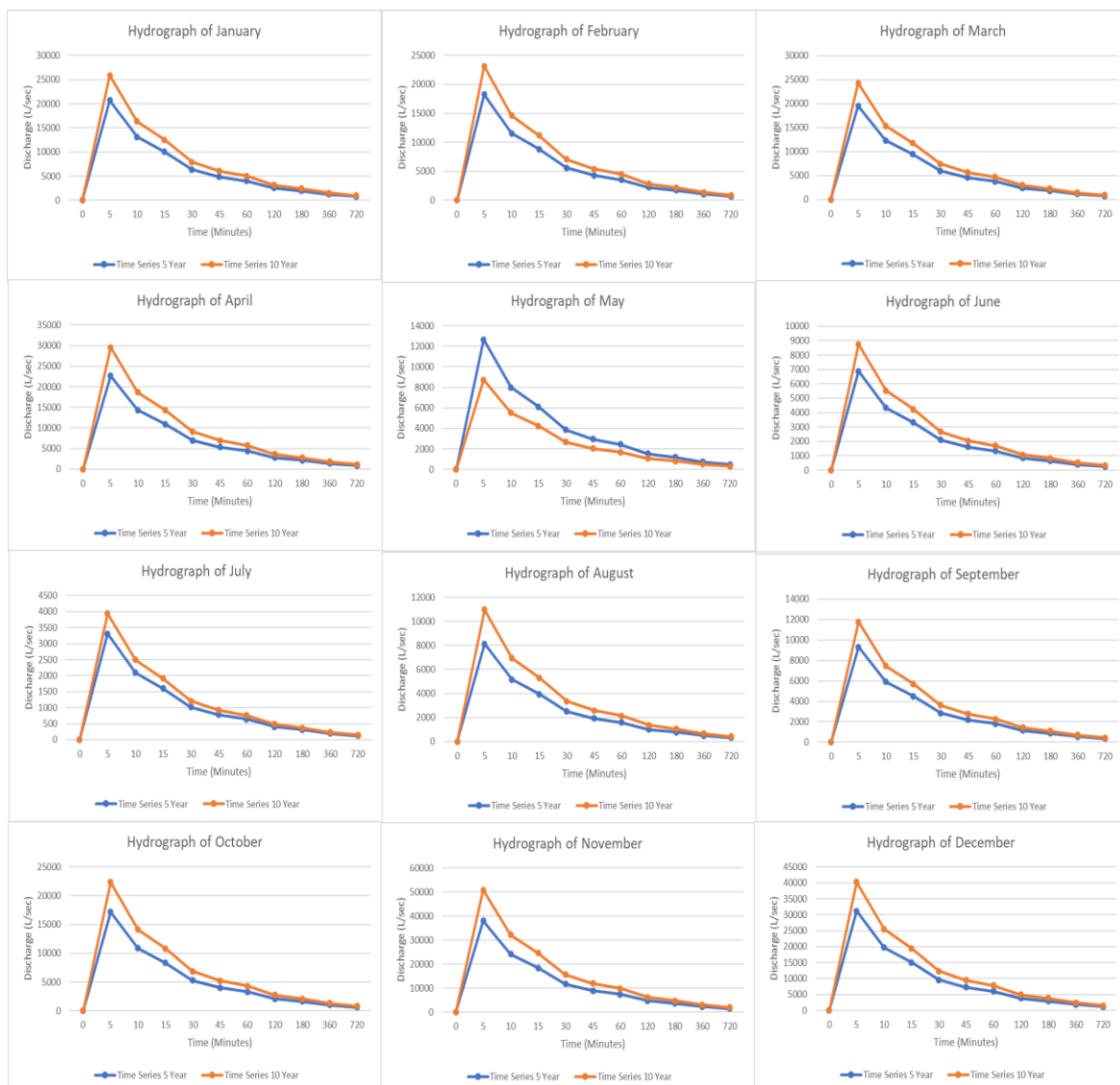


Figure 4. Hydrograph curve for estimating peak discharge in Central Citarum Zone.

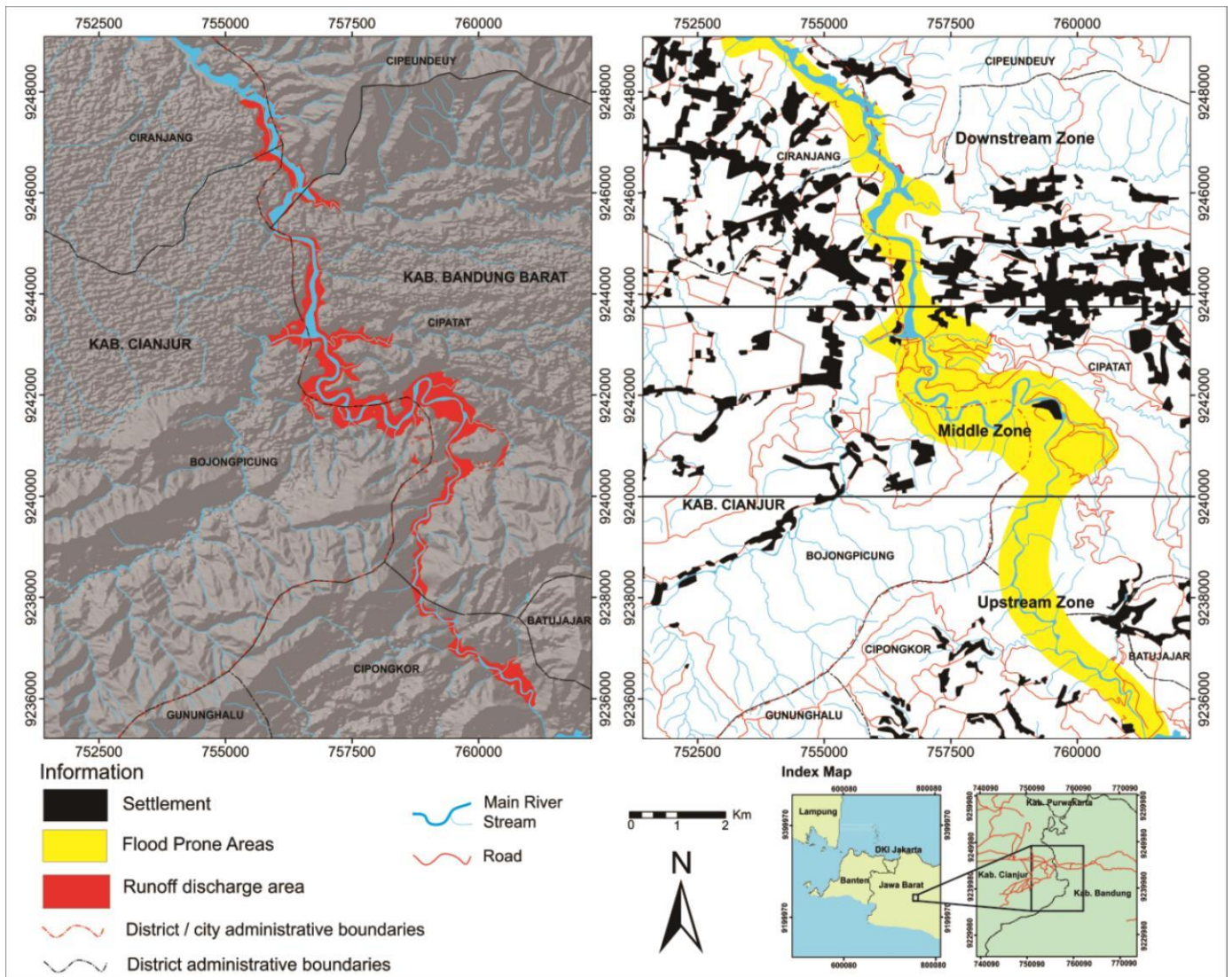


Figure 5. Map of flood simulation has been created using HEC-RAS software and overlay with DEM (left) and flood prone delineation of the study area (right).

4. Conclusion

Based on the data that has been processed, it shows that the rainfall with the highest intensity occurred in November with a value of 448.07 mm/hour, and the lowest intensity was in July with a value of 52.50 mm/hour. The Intensity Duration Frequency (IDF) curve provides information that rainfall with high intensity has a relatively short duration than rainfall with low intensity, which has a longer duration. The lithology type parameter is very influential in this study, which supports a large coefficient value. The simulation results show an increase in flow rate reaching 11.2%, which means it affects the river's capacity to accommodate the overflow load. The study area's simulation map of flood-prone areas is divided into three segments, namely the upstream segment, the middle segment, and the downstream segment, which are based on the level of flood vulnerability in the study

area. The upstream part has a low hazard, the middle segment has a high hazard, and the downstream segment has a low hazard.

Acknowledgement

The publication was funded by PNPB, Faculty of Engineering, Universitas Sriwijaya, year 2021. SP DIPA-023.17.2.677515/2021, on November 23, 2020. In accordance with the Rector's Decree Number: 0315/UN9.FT/TU.SK/2021, on May 5, 2021. The author also expressed great appreciation for Budhi Setiawan, PhD. for substantial discussion.

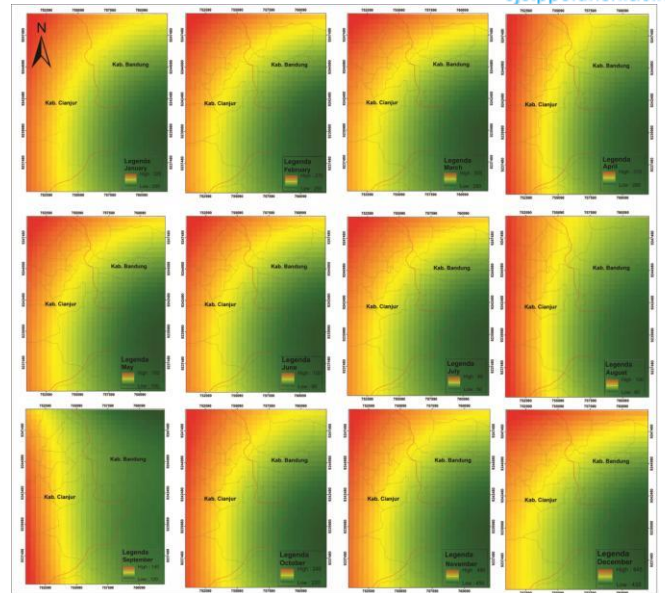
References

- [1] D. Harlan, I. K. Hadihardaja, A. A. Kuntoro, Enung,

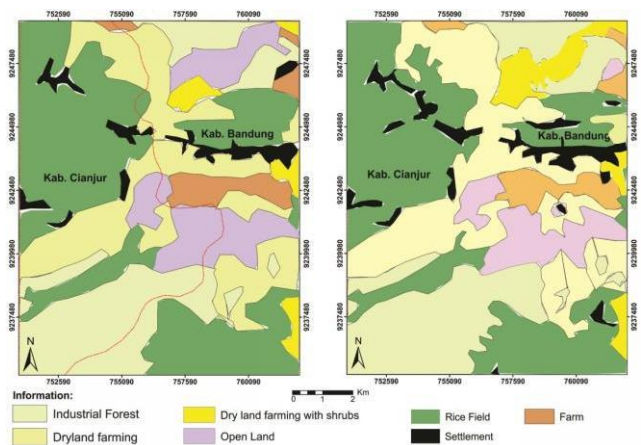
- and D. Faturachman, "Derivation of the critical rainfall level needed for an early flood warning in the Upper Citarum river basin Indonesia," *Int. J. GEOMATE*, vol. 14, no. 43, pp. 167–174, 2018, doi: 10.21660/2018.43.50926.
- [2] A. B. Safarina, N. D. Lestari, and D. Aprilianingsih, "Rainfall Threshold of Citarum River Flood for Early Warning on Urban Area Rainfall Threshold of Citarum River Flood for Early Warning on Urban Area," 2021, doi: 10.1088/1755-1315/728/1/012001.
- [3] A. Fortunato, E. Oliveri, and M. R. Mazzola, "Selection of the optimal design rainfall return period of urban drainage systems," *Procedia Eng.*, vol. 89, pp. 742–749, 2014, doi: 10.1016/j.proeng.2014.11.502.
- [4] N. Bezak, M. Šraj, S. Rusjan, and M. Mikoš, "Impact of the rainfall duration and temporal rainfall distribution defined using the Huff curves on the hydraulic flood modelling results," *Geosci.*, vol. 8, no. 2, 2018, doi: 10.3390/geosciences8020069.
- [5] B. Bogatinoska and O. U. Nederland, "Hydrological and Hydraulic Analysis of River Crossings," no. February, 2019.
- [6] A. Faqih, "A Statistical Bias Correction Tool for Generating Climate Change Scenarios in Indonesia based on CMIP5 Datasets," *IOP Conf. Ser. Earth Environ. Sci.*, vol. 58, p. 12051, 2017, doi: 10.1088/1755-1315/58/1/012051.
- [7] M. Jarraud and A. Steiner, *Climate Change Synthesis Report*, Intergover., vol. 9781107025. 2014.
- [8] T. Blume, E. Zehe, and A. Bronstert, "Rainfall-runoff response, event-based runoff coefficients and hydrograph separation," *Hydrol. Sci. J.*, vol. 52, no. 5, pp. 843–862, 2007, doi: 10.1623/hysj.52.5.843.
- [9] R. Ley, M. Casper, and R. Merz, "Characterisation of watersheds by runoff coefficients," vol. 12, no. May, p. 3966, 2010.
- [10] F. Lallam, A. Megnounif, and A. N. Ghenim, "Estimating the runoff coefficient using the analytic hierarchy process," *J. Water L. Dev.*, vol. 38, no. 1, pp. 67–74, 2018, doi: 10.2478/jwld-2018-0043.
- [11] M. H. Z. Nurrachman, I. Sumardi, and T. Lastini, "Land Cover and Groundwater Recharge Changes Study Using Conservation Index in the Highland Ciburial Village, Bandung Regency," *IOP Conf. Ser. Earth Environ. Sci.*, vol. 166, no. 1, 2018, doi: 10.1088/1755-1315/166/1/012036.
- [12] I. A. Popescu-Busan, G. I. Lazar, A. T. Constantin, and S. V. Nicoara, "Hydraulic Computer Analysis of a River Sector under Altered Flowing Regime Due to an Existing Bridge and Suggested Specific Correction Works," *IOP Conf. Ser. Earth Environ. Sci.*, vol. 362, no. 1, 2019, doi: 10.1088/1755-1315/362/1/012148.
- [13] M. Sherif, S. Akram, and A. Shetty, "Rainfall Analysis for the Northern Wadis of United Arab Emirates: A Case Study," *J. Hydrol. Eng.*, vol. 14, no. 6, pp. 535–544, 2009, doi: 10.1061/(asce)he.1943-5584.0000015.
- [14] D. RAES, "Frequency analysis of rainfall data," *Coll. Soil Phys. 30th Anniv. (1983 - 2013)*, p. 42, 2013, [Online]. Available: <http://indico.ictp.it/event/a12165/session/21/contribution/16/material/0/0.pdf>.
- [15] S. Liang and R. Greene, "A high-resolution global runoff estimate based on GIS and an empirical runoff coefficient," *Hydrol. Res.*, vol. 51, no. 6, pp. 1238–1260, 2020, doi: 10.2166/nh.2020.132.
- [16] M. J. Kundwa, "Development of Rainfall Intensity Duration Frequency (IDF) Curves for Hydraulic Design Aspect," *J. Ecol. Nat. Resour.*, vol. 3, no. 2, pp. 0–14, 2019, doi: 10.23880/jenr-16000162.
- [17] S. Burak, A. Bilge, and D. Ulker, "Computation of monthly runoff coefficients for Istanbul," *Therm. Sci.*, vol. 25, no. 2 Part B, pp. 1561–1572, 2021, doi: 10.2298/tsci191102147b.
- [18] N. S. Al-Amri and A. M. Subyani, "Generation of Rainfall Intensity Duration Frequency (IDF) Curves for Ungauged Sites in Arid Region," *Earth Syst. Environ.*, vol. 1, no. 1, 2017, doi: 10.1007/s41748-017-0008-8.
- [19] H. Baghel, H. K. Mittal, P. K. Singh, K. K. Yadav, and S. Jain, "Frequency Analysis of Rainfall Data Using Probability Distribution Models," *Int. J. Curr. Microbiol. Appl. Sci.*, vol. 8, no. 06, pp. 1390–1396, 2019, doi: 10.20546/ijcmas.2019.806.168.
- [20] T. B. Le, A. Khosronejad, F. Sotiropoulos, N. Bartelt, S. Woldeamlak, and P. Dewall, "Large-eddy simulation of the Mississippi River under base-flow condition: hydrodynamics of a natural diffuence-confluence region," *J. Hydraul. Res.*, vol. 57, no. 6, pp. 836–851, 2019, doi: 10.1080/00221686.2018.1534282.
- [21] G. Khosravi, A. Majidi, and A. Nohegar, "Determination of Suitable Probability Distribution for Annual Mean and Peak Discharges Estimation (Case Study: Minab River- Barantin Gage, Iran)," *Int. J. Probab. Stat.*, vol. 1, no. 5, pp. 160–163, 2013, doi: 10.5923/j.ijps.20120105.03.
- [22] M. Agbazo, G. Koton'Gobi, B. Kounouhewa, E. Alamou, and A. Afouda, "Estimación de las curvas IDF de extrema precipitación por escala simple en el Valle Oueme, al Norte de la República de Benín (Africa occidental)," *Earth Sci. Res. J.*, vol. 20, no. 1, pp. D1–D7, 2016, doi: 10.15446/esrj.v20n1.49405.
- [23] E. A. H. El-sayed, N. Water, F. Prediction, D. Hydrologic, and M. Techniques, "Development of

Empirical Formula to Estimate Short Duration Rainfall NILE WATER SCIENCE & ENGINEERING Volume Ten Issue 1,” no. August, 2020.

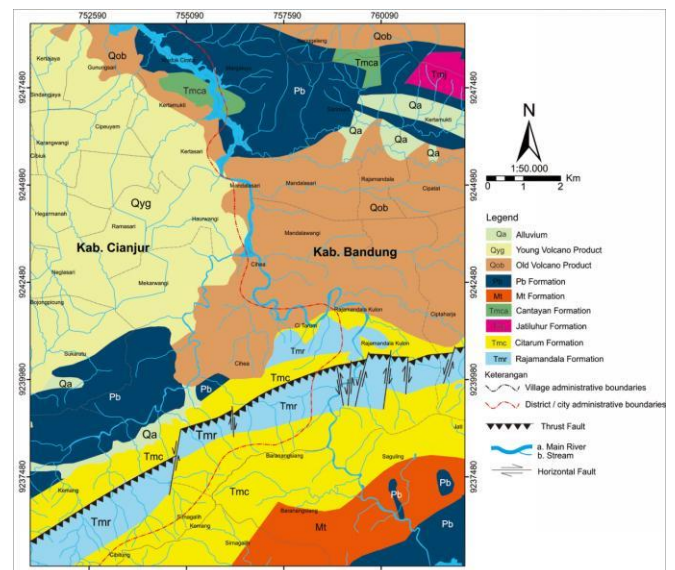
- [24] T. T. Duong, D. M. Do, and K. Yasuhara, “Assessing the effects of rainfall intensity and hydraulic conductivity on riverbank stability,” *Water (Switzerland)*, vol. 11, no. 4, pp. 10–20, 2019, doi: 10.3390/w11040741.
- [25] G. Cristian, R. Beilicci, and E. Beilicci, “Advance Hydraulic Modelling of Maciovitia River, Caras Severin County, Romania,” *IOP Conf. Ser. Mater. Sci. Eng.*, vol. 471, no. 4, pp. 0–6, 2019, doi: 10.1088/1757-899X/471/4/042001.
- [26] A. Moraru, K. R. Usman, O. Bruland, and K. Alfredsen, “River idealization for identification of critical locations in steep rivers using 2D hydrodynamic modelling and GIS,” *22nd North. Res. Basins Work. Symp.*, no. August, pp. 145–154, 2019, doi: 10.13140/RG.2.2.13276.64647.
- [27] J. Ahn, W. Cho, T. Kim, H. Shin, and J. H. Heo, “Flood frequency analysis for the annual peak flows simulated by an event-based rainfall-runoff model in an urban drainage basin,” *Water (Switzerland)*, vol. 6, no. 12, pp. 3841–3863, 2014, doi: 10.3390/w6123841.
- [28] A. Bomers, R. M. J. Schielen, and S. J. M. H. Hulscher, “The influence of grid shape and grid size on hydraulic river modelling performance,” *Environ. Fluid Mech.*, vol. 19, no. 5, pp. 1273–1294, 2019, doi: 10.1007/s10652-019-09670-4.
- [29] M. I. Yuce, M. Esit, and M. C. Karatas, “Hydraulic geometry analysis of Ceyhan River, Turkey,” *SN Appl. Sci.*, vol. 1, no. 7, 2019, doi: 10.1007/s42452-019-0800-1.
- [30] R. Vesipa, C. Camporeale, and L. Ridolfi, “Hydraulics of braided river dynamics. Insights from flume experiments,” *E3S Web Conf.*, vol. 40, pp. 1–8, 2018, doi: 10.1051/e3sconf/20184002020.
- [31] M. K. Bhuyan, “Geo-Hydraulic Performance Evaluation of River Embankments in Geo-Hydraulic Performance Evaluation of River Embankments in Coastal Odisha,” no. March, 2019.



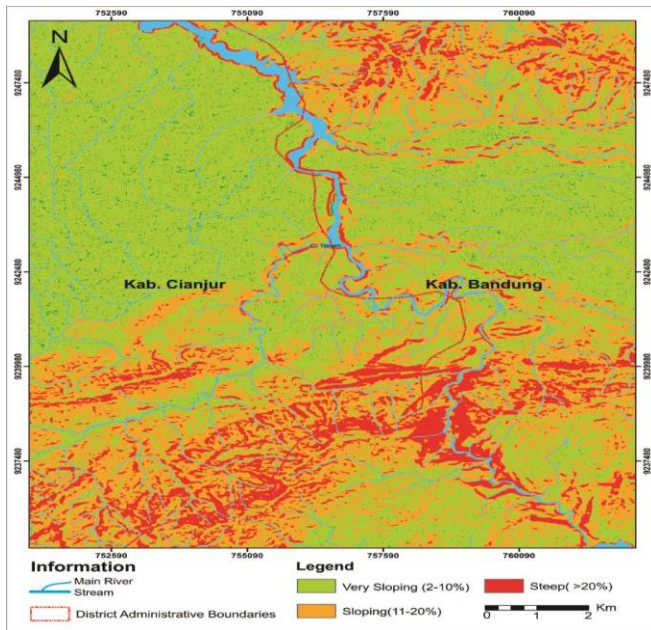
Appendix 1. Rainfall map in the study area.



Appendix 2. Map of the land cover of the study area, 2014 (left) and 2019 (right).



Appendix 3. Geological map of the study area.



Appendix 4. Slope map of the research area.